Available online at www.sciencedirect.com
SCIENCE DIRECT
Geochimica et Cosmochimica Acta 70 (2006) 3855–3868
Geochimica
www.elsevier.com/locate/gca

A numerical model of trace-element coprecipitation in a physicochemical calcification system: Application to coral biomineralization and trace-element 'vital effects'

Daniel J. Sinclair [a,*], Michael J. Risk [b]

[a] GEOTOP, Université du Québec à Montréal, C.P. 8888 Succ. Centre-Ville, Montréal Québec, H3C 3P8, Canada
[b] School of Geography and Geology, McMaster University, Hamilton ON, Canada

Received 9 February 2005; accepted in revised form 30 May 2006

Abstract

A mixed equilibrium/kinetic steady-state numerical model of coral calcification has been developed to test whether a physicochemical calcification mechanism is able to account for recent geochemical observations, in particular correlated trace-element variations presented in a companion paper [Sinclair, D.J., 2005. Correlated trace-element 'vital effects' in tropical corals: a new tool for probing biomineralization chemistry. *Geochim. Cosmochim. Acta* **69** (13), 3265–3284]. The model simulates trace-element partitioning from a $CaCO_3$ supersaturated extracellular calcifying fluid (ECF) which has been modified by enzymatic input of Ca^{2+} and removal of $2H^+$ by CaATPase. CO_2 input is modelled as a diffusion process, while the ECF is continuously replenished by fresh seawater, which is the sole source of minor and trace-elements (TEs). Trace-element species fully equilibrate in the ECF, and selected trace-element species kinetically compete with Ca^{2+} or CO_3^{2-} at the surface of the growing crystal. Each simulation is run to steady-state, and results are presented for a grid of CaATPase ion pumping rates and seawater replenishment rates. The dominant feature of the model output occurs when CaATPase ion pumping is high while seawater replenishment rates are low. At this point, CO_2 diffusion reaches its maximum, C input becomes limiting, buffering capacity is reduced and the pH of the system rises dramatically; significantly affecting the TE composition of the skeleton. At more modest pumping rates, the model reproduces the relative amplitudes of trace-element variations and slopes of the mutually positive correlations between B, Sr and U observed by Sinclair [Sinclair, D.J., 2005. Correlated trace-element 'vital effects' in tropical corals: a new tool for probing biomineralization chemistry. *Geochim. Cosmochim. Acta* **69** (13), 3265–3284], but does not reproduce the negative correlations with Mg. The best fit between model and observation occurs when the coral simultaneously increases ion pumping *and* seawater replenishment rates: a strategy which allows rapid calcification while avoiding dangerously high pH variations. The model predicts that calcification occurs at only moderate pH elevations (8.3–8.4) with seasonal TE variations being explained by a shift of only 0.3 pH units. The model does not reproduce the full amplitude of diurnal pH variations observed recently. Sensitivity tests show that the model output is relatively insensitive to changes in the composition of the fluid from which the ECF is drawn (such as might occur if photosynthesis or active C transport mechanisms significantly modify the penultimate fluid source). Further research, however, is needed to establish the consequences of active transport of TEs and anions to the calcifying site.

1. Introduction

Scleractinian corals precipitate a $CaCO_3$ skeleton and there is no doubt that they biologically manipulate their calcifying environment to enhance the rate of $CaCO_3$ deposition (Goreau, 1959; Goreau and Goreau, 1959; Pearse and Muscatine, 1971; Chalker and Taylor, 1975; Chalker, 1976; Marshall, 1996). The exact mechanism(s) used by the coral to enhance calcification is not fully understood; however, there are two major schools of thought. The first is 'physicochemical calcification', in which the coral skeleton precipitates freely from a pocket of seawater modified by enzymatic ion transport (see reviews in Constantz,

* Corresponding author. Present address: Institute for Geophysics, Jackson School of Earth Sciences, University of Texas in Austin, TX 78759-8500, USA.
E-mail address: djsweb1971@yahoo.com.au (D.J. Sinclair).

0016-7037/$ - see front matter © 2006 Elsevier Inc. All rights reserved.
doi:10.1016/j.gca.2006.05.019

1986; McConnaughey, 1986; McConnaughey, 1989a; Cohen and McConnaughey, 2003). The second is 'organic matrix calcification', in which coral calcification is initiated and controlled by an organic matrix secreted by the coral (see reviews in Johnston, 1980; Allemand et al., 1998; Cuif and Sorauf, 2001; Dauphin, 2001).

Despite these distinct ideas having been well-established for more than 40 years (Goreau, 1959; Barnes, 1970), the dichotomy remains, which seems remarkable, given how fundamentally different these two mechanisms are. In the last few years, driven largely by improvements in microscale analytical methodology, a wealth of new information has become available in the form of physiological studies (Kühl et al., 1995; Allemand et al., 1998; Furla et al., 2000; Al-Horani et al., 2003a,b), structural studies (Clode and Marshall, 2002a; Clode and Marshall, 2003a,b; Perrin, 2003; Cuif and Dauphin, 2004), and geochemical studies (Allison and Tudhope, 1992; Allison, 1996a,b; Sinclair et al., 1998; Cohen et al., 2001; Adkins et al., 2003; Cuif et al., 2003; Meibom et al., 2003; Rollion-Bard et al., 2003a,b; Meibom et al., 2004; Sinclair, 2005).

It is towards the latter which we turn our attention. The growing body of geochemical observations in coral skeletons constitutes an increasingly restrictive set of criteria that any calcification mechanism must meet. This is particularly pertinent for the physicochemical theory of calcification which, being grounded in the principles of inorganic (thermodynamic and kinetic) solution/crystal chemistry, is now at a stage where it may begin to be quantitatively tested against the chemical observations from coral skeleton (McConnaughey, 1989b; Adkins et al., 2003; Sinclair, 2005). If recent chemical observations do not accord with the basic predictions of the numerical models, then this may be the basis for rejecting physicochemical calcification as a possible mechanism of skeleton formation.

Here, we expand on the simpler equilibrium-based model of trace-element coprecipitation presented in Sinclair (2005) that was derived from the mechanism proposed by McConnaughey (1989b). Our model differs from the previous one, being a full kinetic/equilibrium steady-state simulation incorporating kinetic coprecipitation of TEs, and a diffusion boundary-condition for CO_2. The model is implemented in the (freeware) USGS chemical simulation code 'PHREEQC' (Parkhurst and Appelo, 1999), and full input templates and code can be found in the Electronic Annexes.

The output of this model is critically evaluated against recent isotope and trace-element 'vital effects' observed in a range of Scleractinian corals. Specifically, we study whether the model is able to reproduce the mutual correlation slopes and relative amplitudes of seasonal and fine-scale trace-element variations reported by Sinclair (2005).

We do not attempt any modelling of an organic matrix calcification mechanism. At present the chemical implications of such a mechanism are not sufficiently resolved to allow us to construct a falsifiable geochemical hypothesis. Our model, however, represents a conceptual template against which new observations/scenarios can be quantitatively tested, and can potentially be modified to include aspects of biological calcification when, and if, critical numerical data becomes available.

2. Description of model + implementation

2.1. Overview of the model

For the sake of brevity, an overview description of the model is presented here. Full details of the model, and a critical review of the assumptions and parameters used therein, can be found in electronic annex EA-1.

2.1.1. Conceptual model of calcification

This calcification model is based on the 'trans' calcification mechanism proposed by McConnaughey (1986, 1989b) (Fig. 1). Calcification is assumed to occur from within a pocket of solution (the ECF) which is isolated by a calicoblastic membrane. This could be either a pocket of fluid trapped against the skeleton, an intracellular vesicle precipitating aragonite needles in situ, or a crystal nucleated by and growing around a porous organic matrix. The ECF is derived from seawater, but is modified by the coral using the membrane-bound enzyme CaATPase, which actively transports Ca^{2+} into the ECF, exchanging it for $2H^+$ ions to maintain charge neutrality. The effect of this is to raise the Ca^{2+} ion concentration, but also the pH. The high pH shifts the $CO_2/HCO_3^-/CO_3^{2-}$ equilibrium within the system towards CO_3^{2-}, lowering the aqueous CO_2 concentration and therefore initiating a diffusion of CO_2 across the calicoblastic membrane (which is permeable to small neutral molecules).

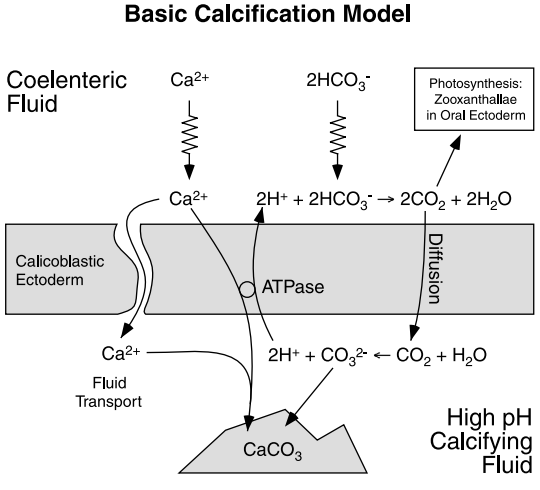

Fig. 1. Schematic of calcification system. In this model, corals calcify by pumping protons from the calcifying fluid in exchange for Ca^{2+} ions from the coelenteron. This raises the pH of the precipitating microenvironment, generating high CO_3^{2-} concentrations and significantly increasing the saturation state of $CaCO_3$. Protons discharged into the coelenteron react with bicarbonate liberating CO_2 which is used for photosynthesis by the zooxanthallae (Modified from McConnaughey and Whelan, 1997).

The coral is assumed to continuously (or periodically) replenish the ECF with fresh seawater removing depleted seawater to maintain a constant volume (Braun and Erez, 2004). Such replenishment is likely as seawater is a rich source of Ca^{2+} for the coral skeleton (being a significant proportion of the total Ca—see McConnaughey, 1989b; Sinclair, 2005 and also below). A seawater source for the ECF is consistent with the relatively indiscriminate incorporation into the coral skeleton of a number of TEs and other chemical species found in the surrounding seawater (Cohen and McConnaughey, 2003; Braun and Erez, 2004).

2.1.2. Trace-elements

The purpose of this modelling is specifically to study the implications of the McConnaughey model of biological ion transport on the composition of coral skeleton. As such, the trace-element coprecipitation mechanism is a simplification of the inorganic precipitation kinetics, and does not include direct temperature and calcification rate influences on element partitioning. Justification and discussion concerning these assumptions is presented in detail in electronic annex EA-1.

In the model, the CaATPase is specific for Ca^{2+}, and the only source of TEs to the ECF is from inputs of seawater. trace-elements are added in the same proportions as average ocean water. Specific aqueous TE species are assumed to compete kinetically with major aqueous ions (Sr^{2+} and Mg^{2+} compete with Ca^{2+}, while $B(OH)_4^-$ and $UO_2(CO_3)_3^{4-}$ compete with CO_3^{2-}). trace-elements are assumed to coprecipitate with constant (invariant) partition coefficients. Full equilibration of all ions within the aqueous solution of the ECF is assumed, but no equilibrium is assumed within the aragonite crystal (solid-state diffusion of ions within the crystal being too slow relative to the elevated precipitation rates to result in an equilibrium solid). For more details, refer to discussion presented in electronic annex EA-1.

The partition coefficients used in this model are arbitrary constants selected to reproduce the average composition of the coral. As such, the model cannot make independent predictions about the TE/Ca ratios in the $CaCO_3$ (as was done in Sinclair, 2005). However, we do not attempt to interpret absolute TE/Ca ratios: the aim of this work is to reproduce the magnitude and slopes of relative changes in TE/Ca ratios. As with any ratio, constant factors cancel, and relative TE/Ca variations are therefore independent of the choice of partition coefficient.

2.1.3. Implementation

The model is set up as a mixed equilibrium/kinetic system within the USGS chemical speciation code PHREEQC (Parkhurst and Appelo, 1999 and see also http://wwwbrr.cr.usgs.gov/projects/GWC_coupled/phreeqc/), using the thermochemical database WATEQ4F with one modification to the speciation of B (see electronic annex EA-1 for details).

Calcium carbonate precipitation is assumed to have an exponential rate-law dependence on the saturation index of aragonite in solution (Zhong and Mucci, 1989). Charge balanced trace-element phases are assumed to coprecipitate at a rate calculated from the product of the calcium carbonate precipitation rate, the partition coefficient, and the activity ratio of the precipitating aqueous species to Ca^{2+} (or CO_3^{2-} in the case of anion substituents) in solution. CO_2 is assumed to diffuse across the calicoblastic membrane at a rate determined by the CO_2 concentration gradient across the membrane and the membrane diffusion constant (McConnaughey, 1989b; Adkins et al., 2003).

PHREEQC cannot simulate a constant flow-through of solution, so the system was instead set up as a large number of 'mini-simulations' where a small but discrete input of fresh seawater was added to the ECF, and allowed to react for a short period of time before another input of seawater. This in fact is what would happen if the coral transported seawater to the calcifying surface as discrete pockets of fluid (e.g. via intracellular vesicles or a periodic tissue pump), but also approximates the case for a continuous flow-through of water provided the timestep for adding discrete volumes of fluid is small.

Trace-element variations in the coral are assumed to result from the shift of one steady-state to another, representing discrete calcification 'regimes' such as a diurnal change from active pumping to non-pumping, or longer timescale fluctuations associated with changes in average light and/or nutrient supply. A steady state assumption is justified because the volume of the ECF is small, and a new steady-state is therefore attained rapidly (typically in a matter of minutes). In the model, a steady state was approximated by iterating the addition/reaction step until an identical solution composition resulted each time. The final steady state of solution was taken to be the mean composition across the addition/reaction step (see Fig. 2).

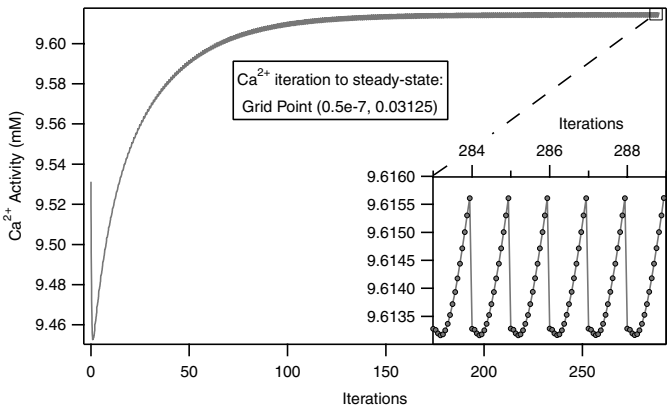

Fig. 2. aCa^{2+} in solution during iteration to steady state. The model was iterated until the calcifying system reached a steady state. As PHREEQC cannot model a flow-through reactor, the steady state was attained by repeatedly adding small packets of seawater fluid and allowing them to react for a short time. The final value graphed in later figures is the average of the fluctuation during the last iteration.

Table 1
Input values for the two independent variables

Independent variable 1	Independent variable 2	
CaATPase pumping rate (mol/m^2/s)	Proportion of ECF replaced each timestep	Time to completely replenish ECF (min)
1.5×10^{-7}		
1.4×10^{-7}	0.5	2
1.3×10^{-7}	0.25	4
1.2×10^{-7}	0.125	8
1.1×10^{-7}	0.0625	16
1.0×10^{-7}	0.03125	32
0.5×10^{-7}	0.015625	64
0.1×10^{-7}		
0.01×10^{-7}		
0.001×10^{-7}		

The model was evaluated for a grid of two independent parameters: (1) CaATPase ion pumping rates (generally referred to as 'pumping') and (2) seawater replenishment rates (generally referred to as 'replenishment'). Values for pumping and replenishment are listed in Table 1.

The values chosen for these independent parameters were partly dictated by the ability of the code to reach a stable numerical solution, but were also sufficient to span a range of scenarios that the coral might naturally encounter. The CaATPase pumping rate ranged from essentially zero up to the point where calcification rates are limited by C transport across the calicoblastic membrane. At the lowest seawater replenishment rate, the ECF was fully replaced by fresh seawater every 64 min—low enough to be insignificant compared with pumping rates. At the highest replenishment rate, the ECF was fully replaced every 2 min, which was sufficiently rapid for seawater DIC to compete with membrane diffusion of CO_2 as a significant source of carbon for the calcifying system.

3. Results

3.1. Calcification system

Graphs of all output parameters in the model discussed below can be found in electronic annex EA-3. The calcification rate is an almost linear function of the rate of ion pumping by CaATPase (Fig. 3 and electronic annex EA-3-1). Calcification rates are generally insensitive to the seawater replenishment rate, tending to decrease slightly as inputs of fresh seawater lower the saturation state of the ECF.

Calcification rates become limited at the highest CaATPase pumping rate and lowest seawater replenishment rate (Fig. 3). This occurs when the concentration of CO_2 in the ECF has dropped to zero (electronic annex EA-3-2), and the CO_2 concentration gradient across the membrane is therefore at a maximum. In this C-supply limited zone, an increase in seawater replenishment results in an increase in calcification, as the seawater represents an additional source of C (as DIC).

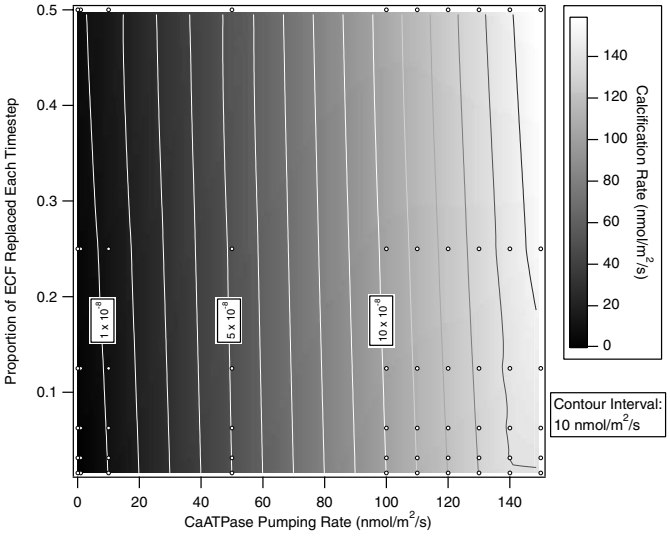

Fig. 3. Model output—calcification rate. This contour plot presents the modelled calcification rate as a function of the two independent variables: CaATPase ion pumping rate (X-axis) and seawater replenishment rate (Y-axis: expressed as a proportion of the ECF replaced during each timestep). Note the point at the bottom right of this figure (see also electronic annex EA-3-1). Here, calcification rates are limited by the diffusion of CO_2 through the membrane (the 'C-supply limiting zone').

The pH of the system increases steadily from 8.2 to around 9.5 as the rate of proton removal by CaATPase pumping increases (Fig. 4 and electronic annex EA-3-3). At the point where C-supply limits the calcification rate, the pH rises very rapidly to values above 11.5. This occurs when the buffering capacity of the HCO_3^-/CO_3^{2-} system becomes depleted as C concentrations drop dramatically (electronic annex EA-3-4) and all C is converted into CO_3^{2-} (electronic annex EA-3-5). In general, the pH of

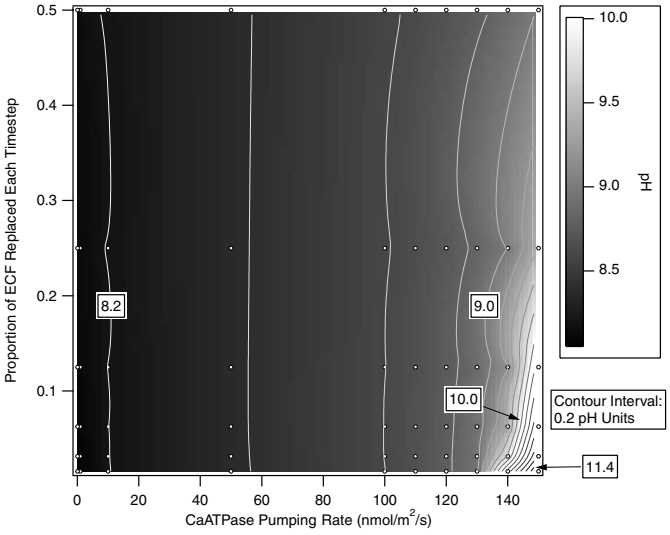

Fig. 4. Model output—pH in the ECF. The contours show the modelled pH as a function of the pumping rate and seawater replenishment rate. See caption for Fig. 3 for further details. Note the rapid rise in pH in the C-supply limiting zone.

the calcifying system is relatively insensitive to seawater replenishment: increasing the input of seawater lowers the pH slightly, except in the C-supply limiting zone where the influence of seawater DIC becomes significant.

Under most conditions, the majority (80–100%) of the C in the ECF (and therefore in the skeleton) comes from CO_2 diffusing across the membrane and only at the very lowest pumping rates does seawater DIC become a dominant source of C (electronic annex EA-3-6). Replenishment of the ECF by fresh seawater lowers the proportion of diffused C—partly because seawater DIC is an alternative C source, but more likely because it lowers the pH, and therefore the CO_2 concentration gradient. Changing the ion pumping rate results in a much bigger change in diffused C. Clearly, establishing a small pH gradient, and thereby initiating CO_2 diffusion, is a highly effective way of boosting the C supply to the ECF.

The proportion of Ca in the ECF supplied by active transport (pumping by CaATPase) varies from 0% (high replenishment, low pumping) up to 100% (low replenishment, high pumping) (electronic annex EA-3-7). In contrast to C, seawater replenishment of the ECF has a much bigger effect on the balance of Ca supply, as seawater is a rich source of Ca^{2+}.

3.2. Major and trace-elements

It is a general prediction of this model that trace-element concentrations in precipitated aragonite will change as the coral modifies its calcification rate. These trace-element changes are driven by:

1. Variations in the aCa^{2+} within the ECF caused by CaATPase pumping.
2. Variations in the aCO_3^{2-} within the ECF caused by changes to the pH (due to proton pumping by CaATPase) and the changing balance of CO_2 diffusion vs $CaCO_3$ precipitation.
3. Variations in the speciation of each trace-element associated with varying pH and aCO_3^{2-}.

The relative importance of each of these factors in controlling the composition of the aragonite differs for each trace-element and varies with pH.

The steady state concentration of Ca in the ECF is generally fairly constant, but increases dramatically in the C-supply limiting zone (high pumping, low replenishment), as its removal rate ($CaCO_3$ precipitation) decreases (Fig. 5 and electronic annex EA-3-8). Away from this zone, Ca concentrations change by only around 4%, and are maximal at mid rates of pumping. This concave-down shape represents a subtly shifting balance between the rates of Ca supply (pumping) and removal (precipitation).

The major control on the steady state CO_3^{2-} concentration in the ECF is the CaATPase pumping rate which directly affects the solution pH and therefore controls the position of

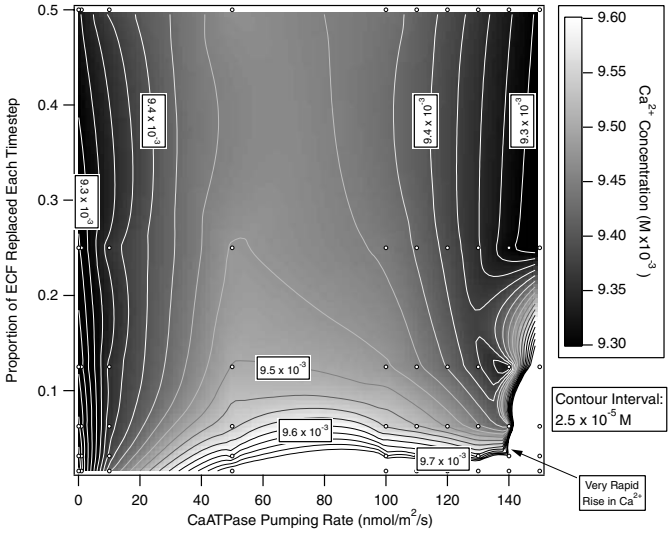

Fig. 5. Model output—Ca^{2+} concentration in the ECF. The contours show the modelled Ca^{2+} concentration in the ECF as a function of the pumping rate and seawater replenishment rate. See caption for Fig. 3 for further details. Note that Ca^{2+} concentrations rise rapidly in the C-supply limiting zone, as calcification rates are limited by the diffusion of CO_2 through the membrane.

the HCO_3^-/CO_3^{2-} equilibrium (electronic annex EA-3-5). In the C-supply limiting zone, the CO_3^{2-} concentration drops sharply. This reflects the sudden decrease in steady state concentration of C_{total} (electronic annex EA-3-4).

The B/Ca ratio in the precipitated $CaCO_3$ drops as pumping rates increase (Fig. 6 and electronic annex EA-3-9), primarily because the solution activity of $B(OH)_4^-$ increases more slowly than CO_3^{2-} as the pH increases. This situation changes at mid pHs: the activity of $B(OH)_4^-$ continues to increase while CO_3^{2-} concentrations become

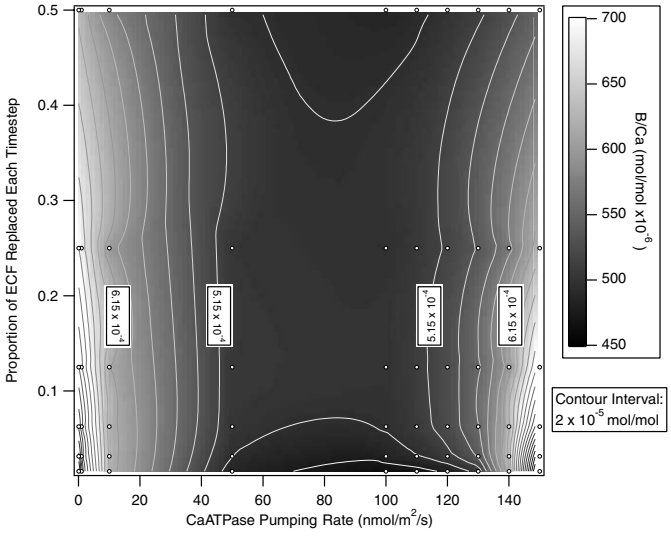

Fig. 6. Model output—B/Ca ratios in the coral skeleton. The contours show the modelled B/Ca ratio in the coral skeleton as a function of the pumping rate and seawater replenishment rate. See caption for Fig. 3 for further details.

limited by C transport. The result is a skeletal B/Ca pattern with a U-shaped minimum at mid pumping rates.

At low replenishment rates, B_{total} and $B(OH)_4^-$ decrease strongly with increasing pumping rates as B-removal (coprecipitation with $CaCO_3$) increases relative to supply. However, this effect is offset in the C-supply limiting zone by the large decrease in CO_3^{2-} which drives a steep rise in the B/CO_3^{2-} (= B/Ca) of the precipitated $CaCO_3$.

The U/Ca ratio in the $CaCO_3$ is a relatively simple function, decreasing evenly towards higher pumping and lower replenishment rates (Fig. 7 and electronic annex EA-3-10). This hides a somewhat complicated solution behaviour where a rapid drop in the activity of $UO_2(CO_3)_3^{4-}$ (caused by a pH-driven shift towards a hydroxylated uranyl species) is partially balanced by the decrease in CO_3^{2-} in the C-supply limiting zone.

Magnesium has a low partition coefficient in aragonite, and the ECF composition is therefore insensitive to changes in the calcification rate. The Mg/Ca ratio in the $CaCO_3$, is therefore relatively constant (Fig. 8 and electronic annex EA-3-11). However, when pHs begin to rise rapidly in the C-supply limiting zone, the Mg/Ca decreases significantly, driven by a shift in aqueous speciation from Mg^{2+} to $Mg(OH)^+$. On a finer scale, the Mg/Ca ratio in the $CaCO_3$ displays a concave-up shape, which is mostly a reflection of the changing aqueous Ca^{2+} concentration (see Fig. 5).

The Sr/Ca in the $CaCO_3$ is relatively sensitive to both seawater replenishment rates and CaATPase pumping rates (Fig. 9 and electronic annex EA-3-12). These changes are largely driven by the Sr concentration in the ECF, which is a balance of supply (seawater input) and removal (Sr coprecipitation with $CaCO_3$) rates. Increasing the rate of pumping results in an increase in the Sr coprecipitation rate, hence a lower steady-state concentration and a reduced Sr/Ca in the skeleton. pH does not affect the Sr composition of the coral: the aqueous speciation of Sr is relatively insensitive to pH, and Sr^{2+} remains the dominant aqueous species from pH 8.1 up to pH 11.

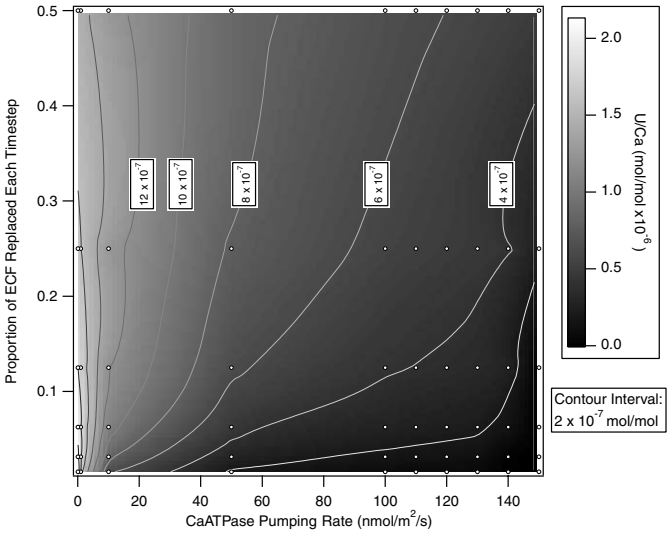

Fig. 7. Model output—U/Ca ratios in the coral skeleton. The contours show the modelled U/Ca ratio in the coral skeleton as a function of the pumping rate and seawater replenishment rate. See caption for Fig. 3 for further details.

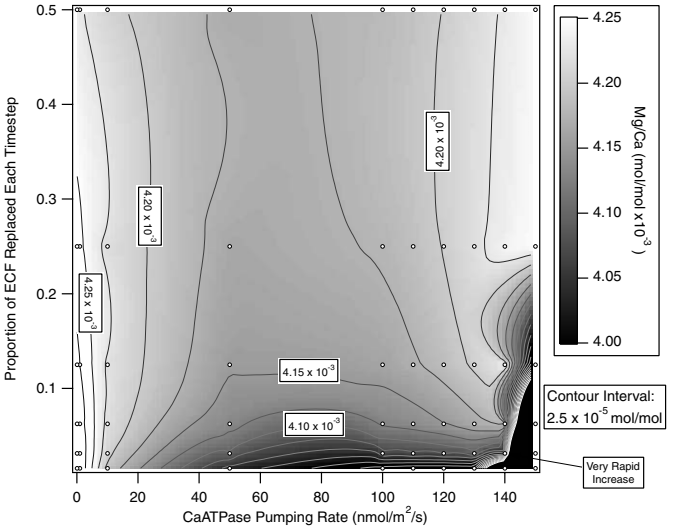

Fig. 8. Model output—Mg/Ca ratios in the coral skeleton. The contours show the modelled Mg/Ca ratio in the coral skeleton as a function of the pumping rate and seawater replenishment rate. See caption for Fig. 3 for further details. Note that for most of the output grid, Mg/Ca ratios do not vary greatly, except in the C-supply limiting zone where they increase very rapidly.

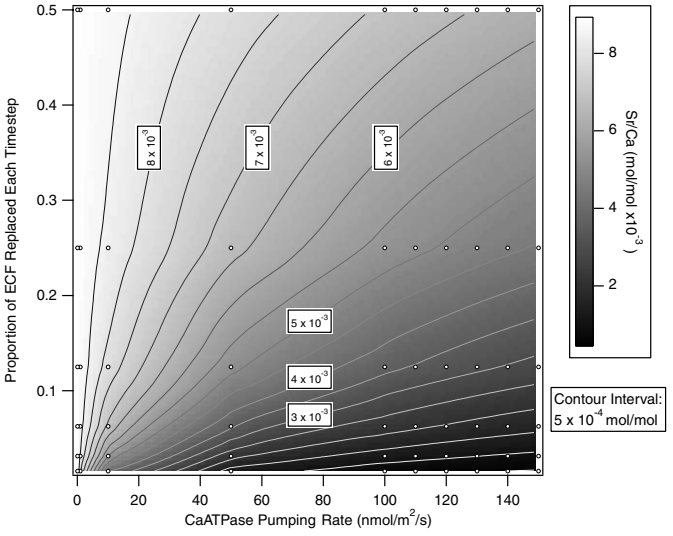

Fig. 9. Model output—Sr/Ca ratios in the coral skeleton. The contours show the modelled Sr/Ca ratio in the coral skeleton as a function of the pumping rate and seawater replenishment rate. See caption for Fig. 3 for further details.

4. Discussion

4.1. Interelement correlations: comparisons with observations

In this model, the coprecipitation rates of all trace-elements are coupled to one biogeochemical mechanism

controlling the rate of skeleton formation. The model therefore predicts that changes in calcification rate will lead to a systematic pattern of correlated trace-element variations. However, there is only one region of the model output where amplitudes and correlation slopes match the observations made by Sinclair (2005).

The amplitude of the seasonal trace-element variations observed by Sinclair (2005) were approximately ±9%, 2%, and 15% for B, Sr, and U, respectively. The amplitudes of fine-scale variations were roughly double this. In the output from this model, correlated variations of this magnitude can be found along one zone ('vector') of the output data, corresponding to a shift from low pumping, low seawater replenishment to moderate pumping, high seawater replenishment (Fig. 10). Profiles of B/Ca, Sr/Ca, and U/Ca variations along this vector are presented in Fig. 11, and it is apparent that the mutual correlations are linear (Fig. 12), as observed for the coral data (Sinclair, 2005).

A negative correlation between TEs and calcification rate (and, therefore, positive interelement correlations) is a general prediction of this model. More rapid calcification is associated with greater input into the system of Ca (pumped by CaATPase) and C (diffusing into the high pH ECF), which tend to 'dilute' the minor trace ions. Thus, the model can be extended to other lattice-substituent ions such as Ba. Barium is a good candidate for a lattice substituent because it forms an isostructural carbonate (witherite) and although it is slightly larger than Ca^{2+} (~25%) the cation site in aragonite tolerates large ions (Speer, 1983). The partition coefficient for Ba in coral aragonite is slightly larger than 1.0 (1.15–1.27—see Lea et al., 1989; Alibert et al., 2003) as is seen for Sr^{2+} (1.0–1.1—see Buddemeier et al., 1981; McCulloch et al., 1994). In this model, therefore, the behaviour of Sr can be taken as an analog for the behaviour of Ba—negatively correlated with calcification rate, and positively correlated with the other elements.

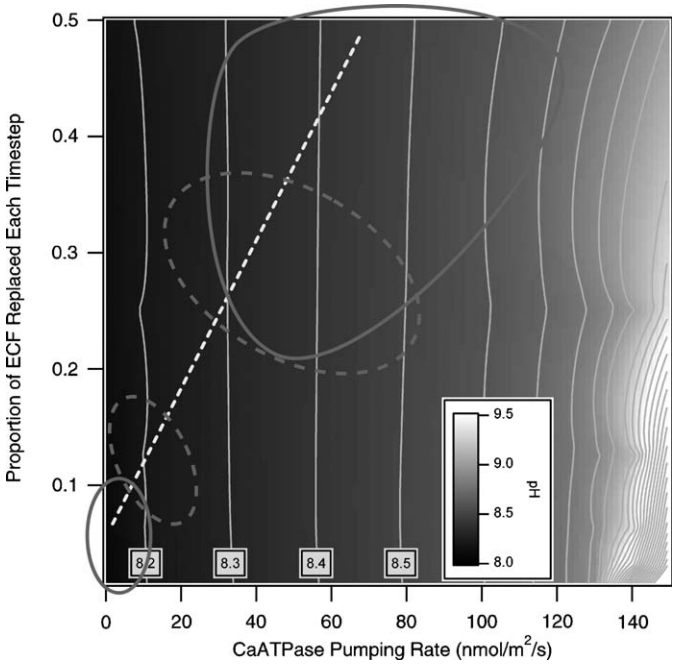

Fig. 10. Matching amplitudes of modelled B, Sr, and U variations to observations. This figure shows the regions of the model output where the correlations between modelled B, Sr, and U match the magnitudes observed in the coral (Sinclair, 2005). The background is an image of the modelled pH (interpolated from the grid of independent variables), with contours in 0.1 pH unit steps. Changes in calcification from the region marked by one solid oval to the other reproduce the magnitude of fine-scale variations in B, Sr, and U. Changes in calcification between the dashed oval regions reproduce the magnitude of seasonal-scale variations. Note that only relatively small changes in pH are involved, and that the coral must increase seawater replenishment at the same time as CaATPase pumping. Line profiles along the vector represented by the dashed line are presented in the following figures.

The negative correlation between Mg/Ca and the other TEs remains a problem, however. Mg/Ca variations observed in the coral are relatively large (±30% for fine-scale or ±15% for seasonal-scale variations). In the model, the predicted Mg/Ca variation in the skeleton is relatively small—around 7% across most of the output grid. Only in the C-supply limiting zone are the model Mg/Ca variations as large as observed in the coral. However, in this zone of the output grid, B/Ca, U/Ca, and Sr/Ca variations are much larger than observed in the coral, and are positively—not negatively—correlated with Mg/Ca. Thus, this model, like the simpler version presented in Sinclair (2005), cannot reproduce the negative Mg/Ca correlations seen in the corals.

The kinetic model for Mg coprecipitation is built upon the assumption that Mg^{2+} substitutes for Ca^{2+} in a cation lattice site. This is not realistic: Mg^{2+} is a small cation which does not fit well into the large aragonite cation site (see electronic annex EA-1 for further discussion). It is more likely that Mg^{2+} is occluded into lattice defects. As defects would increase with increasing calcification rate, Mg^{2+} and calcification rate would be positively correlated. An alternative explanation could be that Mg^{2+} is controlled by some crystallographic factor (see discussion in Sinclair et al., 2005), or that Mg^{2+} is associated with a periodically cycling organic phase (as suggested by Meibom et al., 2004; although, this raises further questions about its strong anti-correlation with U—see Sinclair, 2005).

4.2. Calcification rates

It is difficult to compare the output of this model with calcification rates observed in corals. The model simulates calcification per unit microscopic area (per unit of crystal/membrane surface area), while most calcification rates are determined per unit mass (skeleton or tissue) or macroscopic surface area. The ratio of macroscopic to microscopic area is not well constrained in corals, but was estimated to be between 10 and 100 $m^2_{(microscopic)}/m^2_{(macroscopic)}$ (Johnston, 1980; Gladfelter, 1982, 1983).

This allows a first order comparison to be made: Lough and Barnes (1997) report an average calcification rate for GBR corals of 1.72 g/cm^2/year or 5.4×10^{-6} mol/s/$m^2_{(macroscopic)}$. Assuming 100 $m^2_{(microscopic)}/m^2_{(macroscopic)}$,

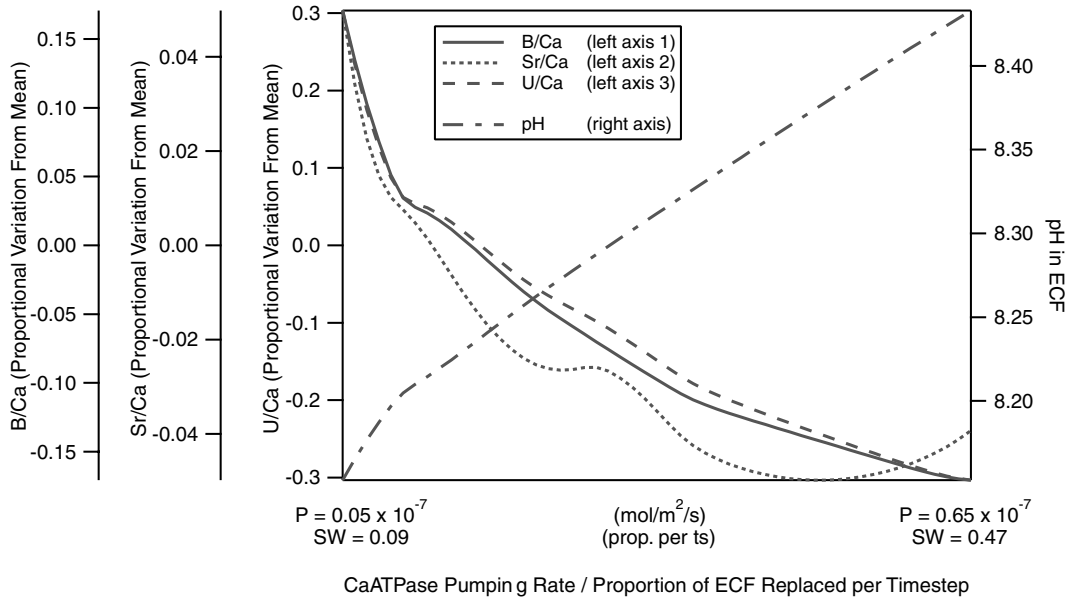

Fig. 11. Line profiles taken along the vector in Fig. 10. Line profiles of modelled B, Sr, and U variation are presented to demonstrate the interelement correlations. Along the vector indicated in Fig. 10, not only are the magnitudes of the B, Sr, and U variation observed by Sinclair (2005) reproduced, but the shape of their variation is similar, resulting in a straight-line correlation in 3D (see Fig. 12). Variations and discontinuous slopes (especially those for Sr) are artefacts of the interpolation method.

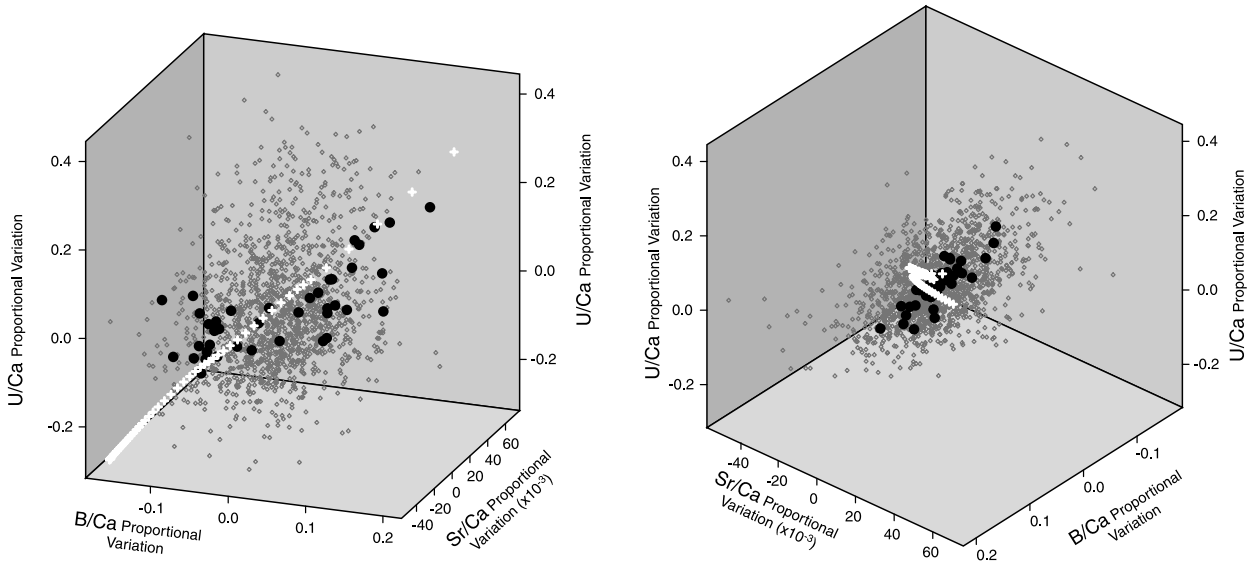

Fig. 12. 3D scatter plot of B, Sr, and U showing model output and observations. This scatter plot displays the modelled interelement correlations for B, Sr, and U plotted against the correlated trace-element data presented in Sinclair (2005). Grey triangles, fine-scale observations. Black dots, seasonal-scale observations. White crosses, modelled variation in B, Sr, and U (along the vector plotted in Fig. 10). Two rotations of the dataset are shown: the second view is approximately down the first principal component of the seasonal-scale correlation in B, Sr, and U.

this would translate to 54×10^{-9} mol/s/m$^2_{(\text{microscopic})}$. By comparison, the average calcification rate in the model is about 40×10^{-9} mol/s/m$^2_{(\text{microscopic})}$ (see Section 4.1). This is a reasonable agreement given the uncertainties in scaling microscopic to macroscopic rates.

The average inter-annual variability in calcification rates for GBR corals is around ±28% of the mean (Lough and Barnes, 1997). In the model, the seasonal amplitude of the trace-element cycles can be reproduced by inter-annual calcification rate changes ranging from about ±16% up to ±100%. Thus, the model is able to reproduce the observed summer-to-winter changes in calcification rate, but generally predicts larger variations. The amplitude of the fine-scale (weekly to monthly) trace-element variations is reproduced in the model by calcification rates changing from almost zero up to >3× average rates. At present it is not known how this corresponds with actual short timescale variations in coral calcification rate.

4.3. pH and stable isotopes

4.3.1. Average pH

One of the most important results of this modelling is the fact that the trace-element variations do not imply calcification at high pH. The model reproduces observed trace-element amplitudes and correlations at only a modest elevation in average pH (roughly 8.3–8.4), while the amplitude of seasonal cycles only requires variations of ±0.15 pH units. This tentatively supports the conclusions of Reynaud et al. (2004) who report minimal offset between calculated and observed $\delta^{11}B$ in corals cultured at different pHs. While those authors conclude that there is no biological mediation of pH, the uncertainty in B isotope fractionation constants does not preclude a modest physiological pH elevation. If physiological pH deviations are small and stable, it may be possible for corals to faithfully record external variations in seawater pH, as suggested by Zeebe et al. (2003) for foraminifera.

4.3.2. Diurnal pH variations and stable isotope fractionation

Diurnal pH variations inferred from high resolution B isotope studies (Rollion-Bard et al., 2003a,b) and measured in the calcifying fluid (Risk and Kramer, 1981; Al-Horani et al., 2003a) are large: ranging from around 7.1 to 9.0. In contrast, the fine-scale TE variations seen by Sinclair (2005) can be reproduced by the model for pHs ranging from a maximum of 8.1 (almost no calcification) up to a maximum of 8.5 (rapid calcification) (see Fig. 11).

This discrepancy can be partly resolved by the coarse size of the laser beam (60 μm diameter) which is insufficient to resolve daily deposits within the coral. Higher resolution measurements of Sr/Ca made by ion microprobe do show a larger amplitude (Allison et al., 2001; Cohen and McConnaughey, 2003; Cohen and Sohn, 2004). However, Sr/Ca ratios in the model are relatively sensitive to pH, and even these larger amplitude variations can be reproduced with pHs no higher than 8.7. At the lower pH, the model cannot reproduce calcification at pHs significantly below ambient seawater (approximately 8.1). Thus there exists a contradiction between the model and the measurements. If large-amplitude pH variation and/or low pH calcification is confirmed, then the theoretical basis of this model may need to be re-examined.

Adkins et al. (2003) observed anomalous C + O isotope variations (where isotopes plot off the linear $\delta^{13}C$ vs $\delta^{18}O$ trend) in the opaque trabecular centers of septae in the deep-sea coral *Desmophyllum*. Their preferred explanation is that these deviations from linearity occur when C membrane transport reaches a maximum (which corresponds to the C-supply limiting case described in Section 3.1). Here, the $\delta^{13}C$ reaches a minimum while further pH increases continue to drive the O isotope fractionation.

Our model predicts that the C-supply limiting case is characterised by very high pHs (>9.5) and extreme depletions in U, Sr, and B. These extreme trace-element variations have not been observed by Sinclair (2005) or others (Allison et al., 2001; Cohen and McConnaughey, 2003), and argues against an equilibrium explanation for stable isotope vital effects. It is possible that current analytical methodology has not yet resolved these regions within the skeleton or that equivalent structures do not exist in *Porites* corals. However, it would seem that high pH, C-diffusion limited calcification is unlikely as high pHs (>10) can disrupt cell membranes (Mendonca et al., 1994; Sampathkumar et al., 2003) and damage tissue, while attempting to calcify while C diffusion is limiting wastes energy resources on futile CaATPase pumping which has little effect on the calcification rate (Fig. 3).

4.4. Photosynthesis and ion transport

4.4.1. Ion diffusion into the coelenteron

The ion transport mechanism used for this model is a necessary simplification of the complex dynamics of ion and carbon transport through the coral tissues. The model assumes that calcifying fluid is drawn from a seawater-composition reservoir, and that the only actively transported ions are Ca^{2+} and H^{+}. In reality, the penultimate source of ions is the coelenteron.

The coelenteron is a semi-isolated pocket of fluid: freely exchanging with seawater when the mouth of the coral is open, but isolated when it is closed. Several authors have suggested that the ingestion of fresh seawater is infrequent,

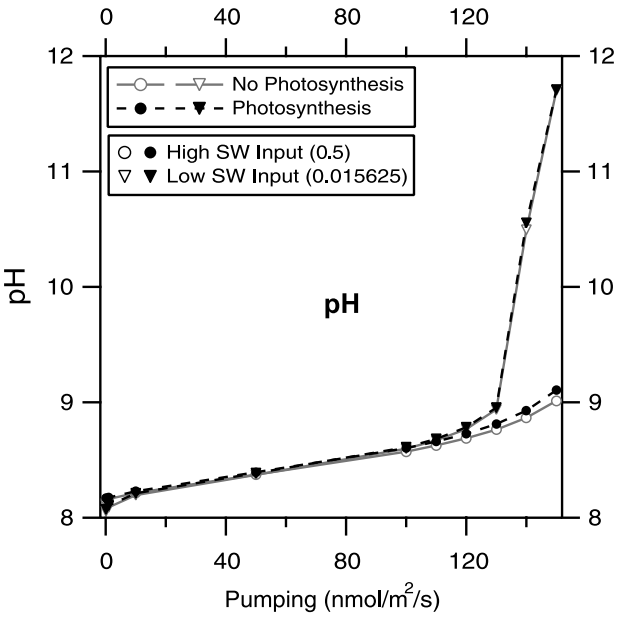

Fig. 13. Effect of photosynthesis on the model pH. This figure shows the effect on the steady-state pH of changing the seawater composition to simulate photosynthetic modification of the coelenteric fluid. Outputs from a 'normal' coelenteron (solid trace) and a photosynthetically modified coelenteron (dashed trace) are graphed. Two lines of the output grid are shown corresponding to low (triangles) and high (circles) seawater replenishment rates. Photosynthesis has almost no effect on the steady-state pH.

and that Ca^{2+} and C must be transported through oral tissues in order to maintain calcification (Wright and Marshall, 1991; Benazet-Tambutte et al., 1996; Furla et al., 1998). Measurements of diffusion across oral tissues (Benazet-Tambutte et al., 1996) suggest that small but significant differences exist in the rates that various ions are transported. If the coelenteron is isolated for extended periods of time, the relative TE abundances may begin to drift away from that of seawater.

The degree to which the trace-element ratios within the coelenteron deviate from seawater will depend on the frequency that the coelenteron is refreshed with seawater and the balance between the precipitation of ions into the skeleton and the diffusion of ions across the oral tissues. If seawater replenishment is frequent, or if diffusion across the oral tissues is fast relative to the removal of ions (by coprecipitation), the trace-element composition of the coelenteron will remain close to the composition of seawater. Benazet-Tambutte et al. (1996) and Furla et al. (2000) suggest that passive ion diffusion is easily fast enough to sustain calcification, which validates the first-order approximation of a seawater-composition coelenteron. With the exception of Ca^{2+}, which may be actively transported to the coelenteron, Clode and Marshall (2002b) did not find significant differences in the Na, Mg, Cl, K, and Sr concentrations in internal seawater compartments compared with standard seawater.

4.4.2. Impact of photosynthesis and respiration

Recent work suggests that the pH, Ca^{2+}, and DIC concentrations of the coelenteron vary in response to the balance of respiration, photosynthesis, and calcification (Kühl et al., 1995; Al-Moghrabi et al., 1996; Furla et al., 1998; Furla et al., 2000; Marshall and Clode, 2002; Al-Horani et al., 2003b; Marshall and Clode, 2003). Al-Horani et al. (2003b) measured daytime Ca^{2+} concentrations which were up to 7% lower than ambient seawater (reduced by calcification), and a pH that was higher—around 8.5—presumably caused by photosynthetic uptake of protons.

It is hard to predict the likely consequences of these mechanisms for the model: raising the coelenteric pH will reduce the CO_2 and HCO_3^- concentration (shifting the equilibrium towards CO_3^{2-}). This, in turn, will lower the gradient between the coelenteron and a calcifying fluid, resulting in a slower C diffusion. On the other hand, higher pHs would lead to elevated CO_3^{2-} concentrations in the ECF, which could offset the slower C diffusion.

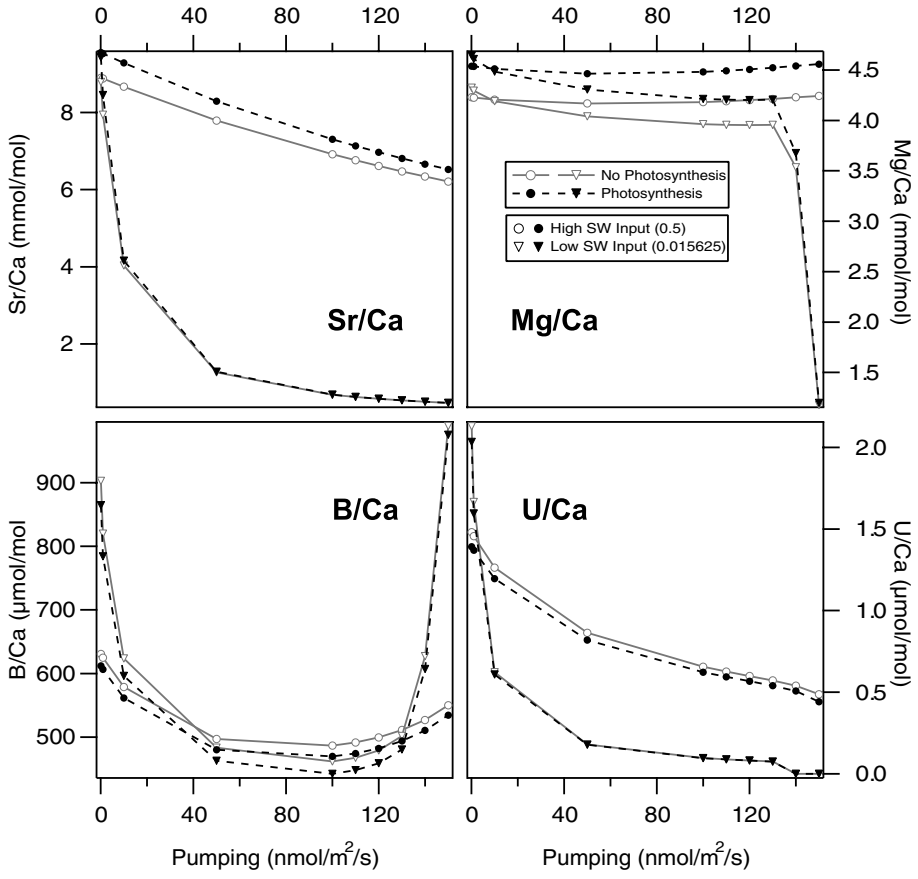

Fig. 14. Effect of photosynthesis on the modelled TE composition. This figure shows the effect on the modelled TE/Ca ratios in the skeleton of changing the seawater composition to simulate photosynthetic modification of the coelenteric fluid. Outputs from a 'normal' coelenteron (solid trace) and a photosynthetically modified coelenteron (dashed trace) are graphed. Two lines of the output grid are shown corresponding to low (triangles) and high (circles) seawater replenishment rates. The effect of photosynthesis is relatively small, and is most pronounced at high seawater input rates and low pumping rates. The differences will have little effect on the conclusions of the model.

In order to test the impact of this on our models, we have repeated several of the simulations so that the ECF is drawn from a solution that has been modified from seawater to simulate the coelenteron measured by Al-Horani et al. (2003b) . The calcium concentration was dropped from 10.3 to 9.6 mM. The effect of photosynthesis (given by the reaction $H^+ + HCO_3^- \rightarrow CH_2O + O_2$) was simulated by removing H_2CO_3 until a pH of 8.5 was achieved. This modified seawater had a lower total C concentration (1.70 mM instead of 1.87 mM), but a slightly higher aragonite saturation index (0.72 instead of 0.59) due to the raised pH.

The output of this modified-coelenteron case is compared with the output from the normal seawater case in Figs. 13 and 14. Photosynthesis makes almost no difference to the steady-state pH of the system (Fig. 13). This means that, in general, the changes to the TE composition of the precipitated aragonite are also relatively small, and do not significantly change the interpretation of the model. At high seawater replenishment and low pumping rates, the cation substituents Mg and Sr are higher by around 7%, reflecting the decreased Ca concentration. This increase becomes smaller as seawater replenishment is reduced, and/or Ca^{2+} pumping rates are increased. At higher pumping or lower seawater input rates the difference between the two simulations becomes negligible.

The anion substituents B and U are even less affected; again the largest differences occur at high seawater replenishment and low pumping rates. In this case, however, the steady state CO_3^{2-} concentration is controlled more by the pH, which is almost identical in the two scenarios. Thus, the steady-state $B(OH)_4^-/CO_3^{2-}$ and $UO_2(CO_3)_3^{4-}/CO_3^{2-}$ ratios are very similar in the two scenarios.

Overall, the effect of a photosynthetically modified coelenteron is minor. The slopes of the B, Sr, and U interelement correlations will, in general, be a little steeper, meaning that a smaller pH change is required to generate the amplitude of variations observed. The exact location of the zone on the output grid where predicted and observed correlations match may also change slightly, but not sufficiently to change the interpretation. This is in agreement with Cohen and McConnaughey (2003) who concluded that photosynthesis does not significantly influence the geochemistry of calcification.

4.4.3. Active transport of ions

Active transport of ions other than Ca^{2+} will affect the applicability of the model, which assumes a fixed transport ratio of trace ions (at seawater composition). There has been some tentative evidence for other ATPases being active in the coral (Krishnaveni et al., 1989; Ip and Lim, 1991; Marshall, 1996), and there is an—as yet unresolved—debate about whether Sr^{2+} is transported by coral CaATPase (Chalker, 1976; Ip and Krishnaveni, 1991; Ip and Lim, 1991; Ferrier-Pagès et al., 2002).

Ip and others (Ip and Krishnaveni, 1991; Ip and Lim, 1991) suggest that CaATPase is selective for Ca, although Ferrier-Pagès et al. (2002) recently came to the opposite conclusion based on the observation that verapamil (a CaATPase inhibitor) inhibited the skeletal uptake of ^{85}Sr with the same IC50 as for Ca uptake. While the authors interpreted this as indicating a common ion transport pathway, an alternative explanation is possible: Sr is a coprecipitated phase and its deposition rate is therefore directly linked to the rate of $CaCO_3$ deposition. Inhibiting Ca transport would therefore inhibit the Sr coprecipitation rate proportionally, even if Sr was derived from a seawater source, and not the CaATPase pathway. Further research will be required to clarify this matter.

Active transport of C to the calcifying space is a more significant issue. This model assumes diffusion of CO_2 from an atmospheric-composition reservoir, whereas recent evidence points towards active transport of HCO_3^- across the calcifying epithelium (Furla et al., 2000 and references cited therein) with C concentrating mechanisms and strong internal cycling changing the C composition of the coelenteric fluid.

The sensitivity of the model to active C transport was tested by increasing the C concentration of the seawater by 20% to simulate some degree of active concentration. The model output (Figs. 15 and 16) shows that the model is relatively insensitive to moderate changes in C: almost no change in pH is observed, while a 20% increase in C

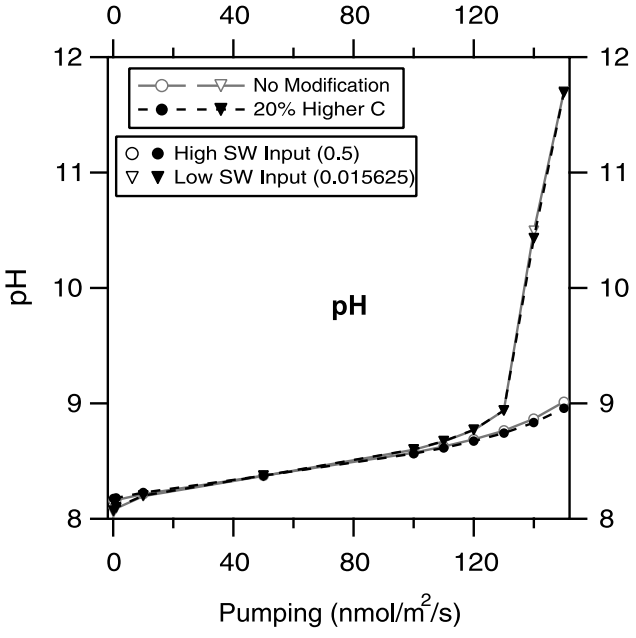

Fig. 15. Effect of raising the C concentration on the model pH. This figure shows the effect on the steady-state pH of increasing the SW C by 20% to simulate some degree of active C concentration by the coral. Outputs from a 'normal' coelenteron (solid trace) and a CO_2 enriched coelenteron (dashed trace) are graphed. Two lines of the output grid are shown corresponding to low (triangles) and high (circles) seawater replenishment rates. Changing the C concentration of the seawater has almost no effect on the steady-state pH in the ECF.

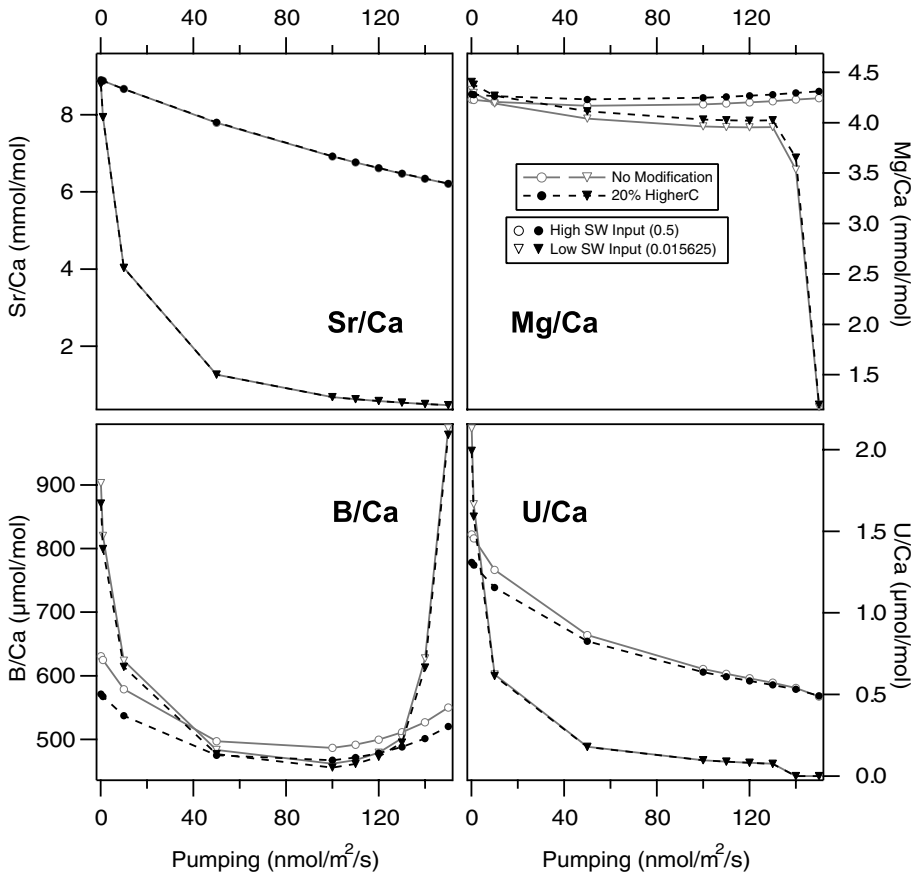

Fig. 16. Effect of raising the C concentration on the modelled TE composition. This figure shows the effect on the modelled TE/Ca ratios in the skeleton of increasing the C concentration of the coelenteron by 20% to simulate some degree of active C transport by the coral. Outputs from a 'normal' coelenteron (solid trace) and a CO_2 enriched coelenteron (dashed trace) are graphed. Two lines of the output grid are shown corresponding to low (triangles) and high (circles) seawater replenishment rates. The model output is relatively insensitive to these changes, with TE/Ca ratios decreasing by at most 12%.

resulted in a maximum decrease in the B/Ca and U/Ca ratios of 10–12% (with this proportion decreasing as pumping rates increased and seawater input rates decreased). Although the model is not particularly sensitive to this parameter, there is no way to know exactly how much the coral might concentrate C. If it does so by orders of magnitude, rather than 10 s of percent, then the model will not be applicable. Further research on active C transport is needed to quantify this parameter.

In future modelling, it might be possible to extend the calcifying system to a three box model, where calcifying fluids are drawn from an intermediate pool (the coelenteron) which is, in turn, modified by inputs from seawater, ion diffusion, active ion transport, photosynthesis, respiration, and calcification. Parameterising this model will, however, be a significant challenge.

5. Conclusions

The physicochemical calcification model presented here predicts that trace-elements will be negatively correlated with calcification rate, and therefore mutually positively correlated. The model reproduces the amplitude and linear correlations of the Sr, B, and U 'vital effects' previously observed at seasonal and short timescales in tropical corals (Sinclair, 2005). The model is not able to reproduce the negative correlation between Mg and the other TEs, and the kinetic model of Mg coprecipitation used here is not believed to be accurate. Mg incorporation may be controlled by an occlusion mechanism, crystallographic factors, or a variable distribution of another phase (such as amorphous $CaCO_3$ or an organic matrix).

The model predicts that at very high calcification rates, CO_2 diffusion becomes a limiting factor, and calcification under these conditions is characterised by a very rapid rise in the pH of the ECF, and very large reductions in the skeletal concentrations of all the trace-elements modelled (significantly larger than any observations reported in the literature). In reality the corals are not likely to calcify at this extreme, as the high pH would damage tissue, and any expenditure of metabolic energy for active transport of ions would be wasted as C diffusion rates limit the calcification rate.

The region of the model output where the Sr, B, and U correlations match observations represents calcification enhancement along a 'vector' of mutually increasing CaATPase pumping and replenishment of the ECF with fresh seawater. This calcification strategy represents an optimal balance allowing rapid calcification while avoiding

the case where C diffusion is limiting and pHs are extreme. Calcification rate increases are associated with relatively mild pH increases (the large-amplitude short-timescale variations can be reproduced with a pH range of 8.1–8.7). The model is not able to reconcile the amplitude of diurnal pH variations reported in the literature with observations of trace-elements, and this might indicate a gap in our understanding of coral calcification.

Variations in the composition of the coelenteron caused by the shifting balance of photosynthesis and calcification (lower Ca^{2+}, lower C, higher pH) are shown to have only a minor impact on the trace-element composition of the coral, being secondary to changes in the rates of CO_2 diffusion, ECF replenishment, and Ca^{2+} pumping. The effect of an active C transport mechanism could be more significant, and further research needs to be undertaken to confirm and quantify this effect.

Overall, it is concluded that a physicochemical calcification model can explain many of the trace-element observations of coral skeleton, and cannot be falsified on the basis of correlated trace-element variations. From a purely geochemical perspective, there is no need to invoke the intervention of an organic matrix in the calcifying process.

Acknowledgments

The authors are grateful to P. Clode and D. Barnes for discussions on coral biomineralization, and for P. Brown and D. Parkhurst for help with the development of these models. Logistical support by C. Hillaire-Marcel is appreciated. Thoughtful and thorough reviews by T. McConnaughey, N. Allison, and A. Cohen considerably improved this manuscript. D. Sinclair was supported at GEOTOP by an NSERC grant held my M. Risk.

Associate editor: David Lea

Appendix A. Supplementary data

Supplementary data associated with this article can be found, in the online version, at doi:10.1016/j.gca.2006.05.019.

References

Adkins, J.F., Boyle, E.A., Curry, W.B., Lutringer, A., 2003. Stable isotopes in deep-sea corals and a new mechanism for "vital effects". *Geochim. Cosmochim. Acta* **6**, 1129–1143.

Al-Horani, F.A., Al-Moghrabi, S.M., de Beer, D., 2003a. The mechanism of calcification and its relation to photosynthesis and respiration in the scleractinian coral *Galaxea fascicularis*. *Mar. Biol.* **142**, 419–426.

Al-Horani, F.A., Al-Moghrabi, S.M., de Beer, D., 2003b. Microsensor study of photosynthesis and calcification in the scleractinian coral, *Galaxea fascicularis*: active internal carbon cycle. *J. Exp. Mar. Biol. Ecol.* **288**, 1–15.

Al-Moghrabi, S., Goiran, C., Allemand, D., Speziale, N., Jaubert, J., 1996. Inorganic carbon uptake for photosynthesis by the symbiotic coral-dinoflagellate association II. Mechanisms for bicarbonate uptake. *J. Exp. Mar. Biol. Ecol.* **199**, 227–248.

Alibert, C., Kinsley, L.P.J., Fallon, S.J., McCulloch, M.T., Berkelmans, R., McAllister, F., 2003. Source of trace element variability in Great Barrier Reef corals affected by the Burdekin flood plumes. *Geochim. Cosmochim. Acta* **67** (2), 231–246.

Allemand, D., Tambutté, E., Girard, J.P., Jaubert, J., 1998. Organic matrix synthesis in the scleractinian coral *Stylophora pistillata*: role in biomineralization and potential target of the organotin tributyltin. *J. Exp. Biol.* **201**, 2001–2009.

Allison, N., 1996a. Comparative determinations of trace and minor elements in coral aragonite by ion microprobe analysis, with preliminary results from Phuket, southern Thailand. *Geochim. Cosmochim. Acta* **60** (18), 3457–3470.

Allison, N., 1996b. Geochemical anomalies in coral skeletons and their possible implications for palaeoenvironmental analysis. *Mar. Chem.* **55**, 367–379.

Allison, N., Finch, A.A., Sutton, R., Newville, M., 2001. Strontium heterogeneity and speciation in coral aragonite: Implications for the strontium paleothermometer. *Geochim. Cosmochim. Acta* **16**, 2669–2676.

Allison, N., Tudhope, A.W., 1992. Nature and significance of geochemical variations in coral skeletons as determined by ion microprobe analysis. *Proceedings of the 7th International Coral Reef Symposium Guam* **1**, 173–178.

Barnes, D.J., 1970. Coral skeletons: an explanation of their growth and structure. *Science* **170**, 1305–1308.

Benazet-Tambutte, S., Allemand, D., Jaubert, J., 1996. Permeability of the oral epithelial layers in cnidarians. *Mar. Biol.* **126**, 43–53.

Braun, A., Erez, J., 2004. Preliminary observations on sea water utilization during calcification in Scleractinian corals. *Eos Trans. AGU Fall Meet. Suppl.* **85** (47). Abstract B14B-04.

Buddemeier, R.W., Schneider, R.C., Smith, S.V., 1981. The alkaline earth chemistry of corals. *Proceedings of the Fourth International Coral Reef Symposium Manila* **2**, 81–85.

Chalker, B.E., 1976. Calcium transport during skeletogenesis in hermatypic corals. *Comp. Biochem. Phys. A* **54**, 455–459.

Chalker, B.E., Taylor, D.L., 1975. Light-enhanced calcification, and the role of oxidative phosphorylation in calcification of the coral *Acropora cervicornis*. *Proc. R. Soc. Lond. B* **190**, 323–331.

Clode, P.L., Marshall, A.T., 2002a. Low temperature FESEM of the calcifying interface of a scleractinian coral. *Tissue Cell* **34** (3), 187–198.

Clode, P.L., Marshall, A.T., 2002b. Low temperature X-ray microanalysis of calcium in a scleractinian coral: evidence of active transport mechanisms. *J. Exp. Biol.* **205**, 3543–3552.

Clode, P.L., Marshall, A.T., 2003a. Calcium associated with a fibrillar organic matrix in the scleractinian coral *Galaxea fascicularis*. *Protoplasma* **220**, 153–161.

Clode, P.L., Marshall, A.T., 2003b. Skeletal microstructure of *Galaxea fascicularis* exsert septa: a high-resolution SEM study. *Biol. Bull.* **204**, 146–154.

Cohen, A.L., Layne, G.D., Hart, S.R., 2001. Kinetic control of skeletal Sr/Ca in a symbiotic coral: Implications for the paleotemperature proxy. *Paleoceanography* **16** (1), 20–26.

Cohen, A.L., McConnaughey, T.A., 2003. Geochemical perspectives on coral mineralization. In: Dove, P.M., De Yoreo, J.J., Weiner, S. (Eds.), *Biomineralization*, vol. 54. Mineralogical Society of America, pp. 151–187.

Cohen, A.L., Sohn, R.A., 2004. Tidal modulation of Sr/Ca ratios in a Pacific reef coral. *Geophys. Res. Lett.* **31**, 1–4 (L16310)doi:10.1029/2004GL020600.

Constantz, B.R., 1986. Coral skeleton construction: a physiochemically dominated process. *Palaios* **1**, 152–157.

Cuif, J.-P., Dauphin, Y., 2004. The environmental recording unit in coral skeletons: structural and chemical evidences of a biochemically driven stepping-growth process in coral fibres. *Biogeosci. Discuss.* **1**, 625–658.

Cuif, J.-P., Dauphin, Y., Doucet, J., Salome, M., Susini, J., 2003. XANES mapping of organic sulfate in three scleractinian coral skeletons. *Geochim. Cosmochim. Acta* **67** (1), 75–83.

Cuif, J.-P., Sorauf, J.E., 2001. Biomineralization and diagenesis in the Scleractinian: part I, biomineralization. *Bull. Tohoku Univ. Museum* **1**, 144–151.

Dauphin, Y., 2001. Comparative studies of skeletal soluble matrices from some Scleractinian corals and Molluscs. *Int. J. Biol. Macromol.* **28**, 293–304.

Ferrier-Pagès, C., Boisson, F., Allemand, D., Tambutté, E., 2002. Kinetics of strontium uptake in the scleractinian coral *Stylophora pistillata*. *Mar. Ecol. Prog. Ser.* **245**, 93–100.

Furla, P., Bénazet-Tambutté, S., Jaubert, J., Allemand, D., 1998. Diffusional permeability of dissolved inorganic carbon through the isolated oral epithelial layers of the sea anemone, *Anemonia viridis*. *J. Exp. Mar. Biol. Ecol.* **221**, 71–88.

Furla, P., Galgani, I., Durand, I., Allemand, D., 2000. Sources and mechanisms of inorganic carbon transport for coral calcification and photosynthesis. *J. Exp. Biol.* **203**, 3445–3457.

Gladfelter, E.H., 1982. Skeletal development in *Acropora cervicornis* I. Patterns of calcium carbonate accretion in the axial corallite. *Coral Reefs* **1**, 45–51.

Gladfelter, E.H., 1983. Skeletal development in *Acropora cervicornis*: II. Diel patterns of calcium carbonate accretion. *Coral Reefs* **2**, 91–100.

Goreau, T.F., 1959. The physiology of skeleton formation in corals. I. A method for measuring the rate of calcium deposition by corals under different conditions. *Biol. Bull.* **116**, 59–75.

Goreau, T.F., Goreau, N.I., 1959. The physiology of skeleton formation in corals. II. Calcium deposition by hermatypic corals under various conditions in the reef. *Biol. Bull.* **117**, 1425–1454.

Ip, Y.K., Krishnaveni, P., 1991. The incorporation of strontium ($^{90}Sr^{2+}$) into the skeleton of the hermatypic coral *Galaxea fascicularis*. *J. Exp. Zool.* **258**, 273–276.

Ip, Y.K., Lim, A.L.L., 1991. Are calcium and strontium transported by the same mechanism in the hermatypic coral *Galaxea fascicularis*?. *J. Exp. Biol.* **159**, 507–513.

Johnston, I.S., 1980. The ultrastructure of skeletogenesis in hermatypic corals. In: Bourne, G.H., Danielli, J.F. (Eds.), *International Review of Cytology*, Vol. 67. Elsevier Science and Technology, pp. 171–214.

Krishnaveni, P., Chou, L.M., Ip, Y.K., 1989. Deposition of calcium ($^{45}Ca^{2+}$) in the coral *Galaxea fascicularis*. *Comp. Biochem. Physiol. A* **94** (3), 509–513.

Kühl, M., Cohen, Y., Dalsgaard, T., Jørgensen, B.B., Revsbech, N.P., 1995. Microenvironment and photosynthesis of zooxanthellae in scleractinian corals studied with microsensors for O_2, pH and light. *Mar. Ecol. Prog. Ser.* **117**, 149–172.

Lea, D.W., Shen, G.T., Boyle, E.A., 1989. Coralline barium records temporal variability in equatorial Pacific upwelling. *Nature* **340**, 373–376.

Lough, J.M., Barnes, D.J., 1997. Several centuries of variation in skeletal extension, density and calcification in massive Porites colonies from the Great Barrier Reef: a proxy for seawater temperature and a background of variability against which to identify unnatural change. *J. Exp. Mar. Biol. Ecol.* **211** (1), 29–67.

Marshall, A.T., 1996. Calcification in hermatypic and ahermatypic corals. *Science* **271**, 637–639.

Marshall, A.T., Clode, P.L., 2002. Effect of increased calcium concentration in sea water on calcification and photosynthesis in the scleractinian coral *Galaxea fascicularis*. *J. Exp. Biol.* **205**, 2107–2113.

Marshall, A.T., Clode, P.L., 2003. Light-regulated Ca^{2+} uptake and O_2 secretion at the surface of a scleractinian coral *Galaxea fascicularis*. *Comp. Biochem. Physiol. A* **136**, 417–426.

McConnaughey, T., 1986. Oxygen and carbon isotope disequilibria in Galapagos corals: isotopic thermometry and calcification physiology. Doctoral, University of Washington.

McConnaughey, T., 1989a. ^{13}C and ^{18}O isotopic disequilibrium in biological carbonates: I. Patterns. *Geochim. Cosmochim. Acta* **53**, 151–162.

McConnaughey, T., 1989b. ^{13}C and ^{18}O isotopic disequilibrium in biological carbonates: II. In vitro simulation of kinetic isotope effects. *Geochim. Cosmochim. Acta* **53**, 163–171.

McConnaughey, T., Whelan, J.F., 1997. Calcification generates protons for nutrient and bicarbonate uptake. *Earth Science Reviews* **42**, 95–117.

McCulloch, M.T., Gagan, M.K., Mortimer, G.E., Chivas, A.R., Isdale, P.J., 1994. A high resolution Sr/Ca and $\delta^{18}O$ coral record from the Great Barrier Reef, Australia, and the 1982-83 El Niño. *Geochim. Cosmochim. Acta* **58**, 2747–2754.

Meibom, A., Cuif, J.-P., Hillion, F., Constantz, B.R., Juillet-Leclerc, A., Dauphin, Y., Watanabe, T., Dunbar, R.B., 2004. Distribution of magnesium in coral skeleton. *Geophys. Res. Lett.* **31**, L23306. doi:10.1029/2004GL02131.

Meibom, A., Stage, M., Wooden, J., Constantz, B., Dunbar, R.B., Owen, A., Grumet, N., Bacon, C.R., Chamberlain, C.P., 2003. Monthly strontium/calcium oscillations in symbiotic coral aragonite: Biological effects limiting the precision of the paleotemperature proxy. *Geophys. Res. Lett.* **30** (7), 1418. doi:10.1029/2002GL01686.

Mendonca, A.F., Amoroso, T.L., Knabel, S.J., 1994. Destruction of gram-negative food-borne pathogens by high pH involves disurption of the cytoplasmic membrane. *Appl. Environ. Microbiol.* **60** (11), 4009–4014.

Parkhurst, D.L., Appelo, C.A.J., 1999. *User's guide to PHREEQC (version 2)—a computer program for speciation, batch-reaction, one-dimensional transport, and inverse geochemical calculations*. US Geological Survey Water-Resources Investigations Report 99-4259.

Pearse, V.B., Muscatine, L., 1971. Role of symbiotic algae (zooxanthellae) in coral calcification. *Biol. Bull.* **141**, 350–363.

Perrin, C., 2003. Compositional heterogeneity and microstructural diversity of coral skeletons: implications for taxonomy and control on early diagenesis. *Coral Reefs* **22**, 109–120.

Reynaud, S., Hemming, N.G., Juillet-Leclerc, A., Gattuso, J.P., 2004. Effect of pCO_2 and temperature on the boron isotopic composition of the zooxanthellate coral *Acropora* sp.. *Coral Reefs* **23**, 539–546.

Risk, M.J., Kramer, J.R., 1981. Water chemistry inside coral heads: Determination of pH, Ca and Mg. *Proceedings of the 4th International Coral Reef Symposium, Manilia,* 54.

Rollion-Bard, C., Blamart, D., Cuif, J.-P., Juillet-Leclerc, A., 2003a. Microanalysis of C and O isotopes of azooxanthellate and zooxanthellate corals by ion microprobe. *Coral Reefs* **22** (4), 405–415.

Rollion-Bard, C., Chaussidon, M., France-Lanord, C., 2003b. pH control on oxygen isotopic composition of symbiotic corals. *Earth Planet. Sci. Lett.* **215**, 275–288.

Sampathkumar, B., Khachatourians, G.G., Korber, D.R., 2003. High pH during Trisodium Phosphate Treatment Causes Membrane Damage and Destruction of *Salmonella enterica* Serovar Enteritidis. *Appl. Environ. Microbiol.* **69** (1), 122–129.

Sinclair, D.J., 2005. Correlated trace element 'vital effects' in tropical corals: A new tool for probing biomineralization chemistry. *Geochim. Cosmochim. Acta* **69** (13), 3265–3284.

Sinclair, D.J., Kinsley, L.P.J., McCulloch, M.T., 1998. High resolution analysis of trace elements in corals by laser-ablation ICP-MS. *Geochim. Cosmochim. Acta* **62** (11), 1889–1901.

Sinclair, D.J., Sherwood, O.A., Risk, M.J., Hillaire-Marcel, C., Tubrett, M., Sylvester, P., McCulloch, M.T., Kinsley, L.P.J., 2005. Testing the reproducibility of Mg/Ca profiles in the deep-water coral *Primnoa resedaeformis*: putting the proxy through its paces. In: Freiwald, A., Roberts, J.M. (Eds.), *Cold Water Corals and Ecosystems—Selected Papers from the 2nd International Symposium on Deep Sea Corals*. Springer-Verlag, pp. 1039–1060.

Speer, A.J., 1983. The kinetics of calcium carbonate dissolution and precipitation. In: Reeder, R.J. (Ed.), *Carbonates: Mineralogy and Chemistry*, Vol. 11. Mineralogical Society of America, pp. 145–190.

Wright, O.P., Marshall, A.T., 1991. Calcium transport across the isolated oral epithelium of scleractinian corals. *Coral Reefs* **10**, 37–40.

Zeebe, R.E., Wolf-Gladrow, D.A., Bijma, J., Hönisch, B., 2003. Vital effects in foraminifera do not compromise the use of $\delta^{11}B$ as a paleo-pH indicator: Evidence from modeling. *Paleoceanography* **18** (2), 1043. doi:10.1029/2003PA00088.

Zhong, S., Mucci, A., 1989. Calcite and aragonite precipitation from seawater solutions of various salinities: precipitation rates and overgrowth compositions. *Chem. Geol.* **78**, 283–299.